Paper 7

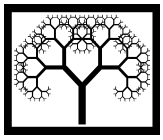

Proceedings of the Eleventh International Conference on Computational Structures Technology,
B.H.V. Topping, (Editor),
Civil-Comp Press, Stirlingshire, Scotland

Calculation of Initial Post-Buckling Behaviour of Moderately Thick Plates using an Exact Finite Strip

S.A.M. Ghannadpour[1], H.R. Ovesy[2]and E. Zia-Dehkordi[2]
[1] Aerospace Engineering Department, Faculty of New Technologies and Engineering, Shahid Beheshti University G.C., Tehran, Iran
[2] Department of Aerospace Engineering and Centre of Excellence in Computational Aerospace Engineering Amirkabir University of Technology, Tehran, Iran

Abstract

An exact finite strip for the buckling and initial post-buckling analysis of moderately thick plates is presented in this paper using first order shear deformation theory (FSDT). In the buckling phase the equilibrium Von-Karman's equation is solved exactly to obtain out-of-plane mode shapes and critical loads. The Von-Karman's compatibility equation is solved exactly in the post-buckling phase with the assumption that the deflected form immediately after buckling is the same as that obtained for the buckling. The principle of minimum potential energy is invoked to solve for the unknown coefficients in the assumed out-of-plane deflection and rotation functions.

Keywords: exact strip, moderately thick plates, initial post-buckling stage, relative stiffness, first order shear deformation theory, Von-Karman's equations.

1 Introduction

Application of plates and plate structures has been increased in many branches of engineering. These structures are often employed to experience in-plane compression loading. Thus, it is important to predict the buckling and post-buckling behaviour of such structures accurately. Since in this paper a new finite strip method (FSM) is utilized to analyse the buckling and initial post-buckling behaviour, it is worth providing a brief review on some of the works done by using FSM.
One of the persons who may be considered as the pioneer is Cheung[1], who first presented the concepts of finite strip method. In the linear buckling field Graves Smith and Sridharan[2] derived the first buckling formulation for isotropic plates under edge load using FSM. Lau and Hancock[3], Wang and Dawe[4] and Zou and Larn[5] have used FSM based on the classical plate theory (CPT), first-order shear deformation theory (FSDT) and higher-order shear deformation theory (HSDT). Many works have been done in the field of geometrically non-linearity based on use of FSM. Early works are those of Graves Smith and Sridharan [6-7]. These

investigators assume a plate with simply supported ends and subjected to progressive end shortening in order to predict the post-buckling behaviour of the structure. An energy-based method, referred to as the semi-energy method by Rhodes and Harvey [8], was first used by Marguerre [9] and has since been used by various researchers. Rhodes[10] and Chou and Rhodes [11] have published several papers on different behaviours of thin-walled structures. The theoretical developments are mostly based on semi-energy method. Ovesy et al [12-14] have developed a semi-energy post-local-buckling FSM (S-e FSM) in which the out-of-plane displacement of the finite strip is the only displacement which is postulated by a deflected form as distinct to that mentioned previously with respect to the semi-analytical FSM (S-a FSM) and Spline FSM. The developed semi-energy FSM (S-e FSM) has been applied to analyze the post-local-buckling behavior of thin flat plates [12], open channel section [13]and box section struts [14]. Ovesy and Ghannadpour [15-18] have developed a full-analytical FSM (F-a FSM) based on CPT in which the Von-Karman's equilibrium equation is solved exactly and thus the buckling mode shapes and loads are obtained with very high accuracy. Then the obtained mode shapes are used in the post-buckling phase and the Von-Karman's compatibility equation is solved exactly and the in-plane displacements are derived.
In this paper for the first time, the theoretical developments of an exact finite strip for the buckling and initial post-buckling analysis of moderately thick plates are presented. The FSDT has been used to model the so-called exact finite strip. The Von-Karman's equilibrium set of equations has been solved exactly with the assumption that the two loaded ends are simply supported and the other two ends have arbitrary out-of-plane boundary conditions. Thus, the general out-of-plane buckling modes are obtained with very high accuracy and then the Von-Karman's compatibility equation is solved exactly to obtain the general form of in-plane displacement field in the post-buckling region. It is necessary to remember that the buckling shape modes obtained from the buckling phase are used as global shape functions for representing the displacement fields in a geometrically non-linear analysis. Thus this method is denoted as full-analytical FSM (F-a FSM) based on first-order shear deformation theory (FSDT).

2 Theoretical developments of the F-a FSM based on FSDT

In this section, the fundamental elements of the theory for the developed exact finite strip in buckling and post-buckling problems are outlined. It must be noted that a perfectly flat exact strip made up of a linear isotropic material (with constant modulus of elasticity E and Poisson ratio ν) is assumed throughout the theoretical developments of this paper. The so-called exact finite strip is assumed to be simply supported out-of-plane at the loaded ends and arbitrary out-of-plane boundary condition at the other two ends. It is important to mention that the plate is assumed to be moderately thick, thus the FSDT is applied in the remaining of the paper.

2.1 Basic formulation of the problem

The exact finite strip, which is schematically shown in Figure 1, is of length L, width b and thickness t. As mentioned earlier, the finite strip is simply supported out-of-plane at both ends, i.e.

$$w = \varphi_y = M_x = 0 \tag{1}$$

It must be noticed that the FSDT is applied, thus

$$\hat{u} = u + z\varphi_x,\ \hat{\upsilon} = \upsilon + z\varphi_y,\ \hat{w} = w \tag{2}$$

where$\hat{u}, \hat{v}$and $\hat{w}$ are components of displacement at a general point, whilst u, v and w are similar components at the middle surface (z=0), φ_x is the rotation of a transverse normal about the axis *y* and φ_y is the rotation of a transvers normal about the axis *x*. On the assumption that the whole transverse shear components can not be neglected in FSDT, the stress-strain relationship at a general point for the plate becomes:

$$\bar{\boldsymbol{\sigma}} = \begin{Bmatrix} \bar{\sigma}_{xx} \\ \bar{\sigma}_{yy} \\ \bar{\tau}_{yz} \\ \bar{\tau}_{xz} \\ \bar{\tau}_{xy} \end{Bmatrix} = \frac{E}{1-\nu^2} \begin{bmatrix} 1 & \nu & 0 & 0 & 0 \\ \nu & 1 & 0 & 0 & 0 \\ 0 & 0 & \frac{1-\nu}{2} & 0 & 0 \\ 0 & 0 & 0 & \frac{1-\nu}{2} & 0 \\ 0 & 0 & 0 & 0 & \frac{1-\nu}{2} \end{bmatrix} . \bar{\boldsymbol{\varepsilon}};\ \ \bar{\boldsymbol{\varepsilon}} = \begin{Bmatrix} \bar{\varepsilon}_{xx} \\ \bar{\varepsilon}_{yy} \\ \bar{\gamma}_{yz} \\ \bar{\gamma}_{xz} \\ \bar{\gamma}_{xy} \end{Bmatrix} \tag{3}$$

where$\bar{\boldsymbol{\sigma}}$and $\bar{\boldsymbol{\varepsilon}}$are the stresses and strains at a general point, respectively.

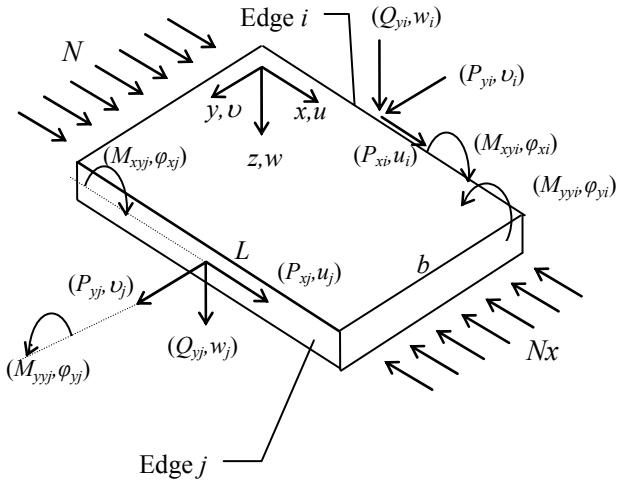

Figure 1: A typical exact finite strip.

Internal forces and moment acting on the edges of a strip are expressed in terms of forces and the moments per unit distance along the strip edge. The forces and moments intensities are related to the internal stress by the equations

$$\left\langle N_{xx} \quad N_{yy} \quad N_{xy} \right\rangle^T = \int_{-h/2}^{h/2} \left\langle \bar{\sigma}_{xx} \quad \bar{\sigma}_{yy} \quad \bar{\tau}_{xy} \right\rangle^T \mathrm{d}z \tag{4a}$$

$$\left\langle M_{xx} \quad M_{yy} \quad M_{xy} \right\rangle^T = \int_{-h/2}^{h/2} \left\langle \bar{\sigma}_{xx} \quad \bar{\sigma}_{yy} \quad \bar{\tau}_{xy} \right\rangle^T z\ \mathrm{d}z \tag{4b}$$

$$\left\langle Q_x \quad Q_y \right\rangle^T = K\int_{-h/2}^{h/2} \left\langle \bar{\tau}_{xz} \quad \bar{\tau}_{yz} \right\rangle^T \, \mathrm{d}z \tag{4c}$$

where K is a shear correction factor which is taken as $\frac{5}{6}$ in the current study. It is noted that the stresses and strains in Equation (3) include the components corresponding to the membrane and bending contributions as outlined below

$$\bar{\boldsymbol{\sigma}} = \boldsymbol{\sigma} + \boldsymbol{\sigma}_b; \quad \bar{\boldsymbol{\varepsilon}} = \boldsymbol{\varepsilon} + \boldsymbol{\varepsilon}_b \tag{5}$$

where $\boldsymbol{\sigma}$ and $\boldsymbol{\varepsilon}$ correspond to the membrane contribution, and $\boldsymbol{\sigma}_b$ and $\boldsymbol{\varepsilon}_b$ relate to the bending and twisting actions. It is noted that the membrane strain $\boldsymbol{\varepsilon}$ can be subdivided into its linear $\boldsymbol{\varepsilon}_l$ and non-linear $\boldsymbol{\varepsilon}_{nl}$ component as given below

$$\boldsymbol{\varepsilon} = \boldsymbol{\varepsilon}_l + \boldsymbol{\varepsilon}_{nl} = \begin{Bmatrix} u_{,x} \\ v_{,y} \\ u_{,y} + v_{,x} \end{Bmatrix} + \begin{Bmatrix} \frac{1}{2}w_{,x}^2 \\ \frac{1}{2}w_{,y}^2 \\ w_{,y}w_{,x} \end{Bmatrix} \tag{6}$$

According to the FSDT the bending strains $\boldsymbol{\varepsilon}_b$ are expressed by the following equations:

$$\boldsymbol{\varepsilon}_b = \langle z\varphi_{x,x} \quad z\varphi_{y,y} \quad z(\varphi_{x,y} + \varphi_{y,x}) \rangle^T \tag{7}$$

Since the potential energy of external loads is zero for the strip under consideration, the total potential energy of the strip V_s is simply equal to the strain energy U_s which is:

$$U_s = \frac{1}{2}\iiint (\bar{\sigma}_{xx}\bar{\varepsilon}_{xx} + \bar{\sigma}_{yy}\bar{\varepsilon}_{yy} + \bar{\tau}_{xy}\bar{\gamma}_{xy} + K\bar{\tau}_{xz}\bar{\gamma}_{xz} + K\bar{\tau}_{yz}\bar{\gamma}_{yz})dxdydz \tag{8}$$

The Von-Karman's equilibrium set of equations and Von-Karman's compatibility equation for large deflections of plate with the assumption that the normal pressure is zero are given by the following equations, respectively:

$$\begin{cases} \frac{1}{2}KA(1-\nu)(w_{,xx} + \varphi_{x,x}) + \frac{1}{2}KA(1-\nu)(w_{,yy} + \varphi_{y,y}) + N_{xx}w_{,xx} + N_{yy}w_{,yy} = 0 \\ D\varphi_{x,xx} + \nu D\varphi_{y,xy} + \frac{1}{2}D(1-\nu)(\varphi_{x,yy} + \varphi_{1y,xy}) - \frac{1}{2}KA(1-\nu)(w_{,x} + \varphi_x) = 0 \\ \nu D\varphi_{x,xy} + D\varphi_{y,yy} + \frac{1}{2}D(1-\nu)(\varphi_{x,xy} + \varphi_{y,xx}) - \frac{1}{2}KA(1-\nu)(w_{,y} + \varphi_y) = 0 \end{cases} \tag{9a}$$

$$\nabla^4 F = E(w_{,xy}^2 - w_{,xx}\, w_{,yy}) \tag{9b}$$

In Equation (9a) A, D are plate stiffness coefficients ($A = \frac{Eh}{1-\nu^2}, D = \frac{Eh^3}{12(1-\nu^2)}$) and N_{xx} is compressive axial load applied in x direction and in Equation (9b) the function F which is known as the Airy stress function is defined as follows:

$$N_{xx} = \frac{\partial^2 F}{\partial y^2}; \qquad N_{yy} = \frac{\partial^2 F}{\partial x^2}; \qquad N_{xy} = -\frac{\partial^2 F}{\partial x \partial y} \tag{10}$$

The positive directions of the edge forces and displacements are shown in Figure 1. It is noted that the in-plane shear force, out-of-plane shear force and bending moment per unit length of the strip edge, i.e. P_x, P_y, Q_y, M_{yy} and M_{xy}, are

$$P_{xi} = -N_{xy}\big|_{y=0}, \quad P_{xj} = N_{xy}\big|_{y=b}, \; P_{yi} = -N_{yy}\big|_{y=0}, \quad P_{yj} = N_{yy}\big|_{y=b} \tag{11}$$

$$Q_{yi} = \frac{1-\nu}{2}\left[KA(w_{,y} + \varphi_y)\right]_{y=0},\ Q_{yj} = -\frac{1-\nu}{2}\left[KA(w_{,y} + \varphi_y)\right]_{y=b}$$

$$M_{yyi} = D\left[\varphi_{y,y} + \nu\varphi_{x,x}\right]_{y=0},\ M_{yyj} = -D\left[\varphi_{y,y} + \nu\varphi_{x,x}\right]_{y=b}$$

$$M_{xyi} = \frac{1-\nu}{2}\left[D(\varphi_{y,x} + \varphi_{x,y})\right]_{y=0},\ M_{xyj} = -\frac{1-\nu}{2}\left[D(\varphi_{y,x} + \varphi_{x,y})\right]_{y=b}$$

The subscripts *i* and *j* denote the corresponding values of forces/displacements at the edges *i* and *j*, respectively. It is noted that in the remaining of the paper, the subscripts $_{0,1,2}$ are used for pre-buckling, buckling and post-buckling stages, respectively.

2.2 Buckling analysis

The out-of-plane buckling deflection mode (w_1), the rotation of a transverse normal about the axis *y* (φ_{1x}) and the rotation of a transverse normal about the axis *x*(φ_{1y}) are obtained by trying to solve the Von-Karman's equilibrium set of equations i.e. Equation (9a). Thus

$$\begin{cases} \frac{1}{2}KA(1-\nu)(w_{1,xx} + \varphi_{1x,x}) + \frac{1}{2}KA(1-\nu)(w_{1,yy} + \varphi_{1y,y}) - N_x w_{1,xx} = 0 \\ D\varphi_{1x,xx} + \nu D\varphi_{1y,xy} + \frac{1}{2}D(1-\nu)(\varphi_{1x,yy} + \varphi_{1y,xy}) - \frac{1}{2}KA(1-\nu)(w_{1,x} + \varphi_{1x}) = 0 \\ \nu D\varphi_{1x,xy} + D\varphi_{1y,yy} + \frac{1}{2}D(1-\nu)(\varphi_{1x,xy} + \varphi_{1y,xx}) - \frac{1}{2}KA(1-\nu)(w_{1,y} + \varphi_{1y}) = 0 \end{cases} \quad (12)$$

In the pre-buckling stage the strip is subjected to the constant compressive axial loads $N_{xx} = -N_x$ and $N_{yy} = 0$. For solving this set of equations it is assumed that the whole three functions are trigonometric in *x* direction and arbitrary in *y* direction:

$$\begin{aligned} w_1(x,y) &= \sin(m\lambda x)\, f_1(y) \\ \varphi_{1x}(x,y) &= \cos(m\lambda x)\, g_1(y) \\ \varphi_{1y}(x,y) &= \sin(m\lambda x)\, s_1(y) \end{aligned} \quad (13)$$

where $\lambda = \pi/L$ and m is the number of half-wavelengths in *x* the direction, $f_1(y), g_1(y)$ and $s_1(y)$ represent the shape functions in the transverse direction *y* for w_1, φ_{1x} and φ_{1y}, respectively. By substituting w_1, φ_{1x} and φ_{1y} from Equation (13) into Equation (12) the following ordinary differential system of equations is obtained:

$$\begin{cases} -Dm^2\lambda^2 g_1 + D(\frac{1+\nu}{2})m\lambda s_1' + D\frac{1-\nu}{2}g_1'' - \frac{1-\nu}{2}KA(m\lambda f_1 + g_1) = 0 \\ Ds_1'' - D(\frac{1+\nu}{2})m\lambda g_1' + D\frac{1-\nu}{2}m^2\lambda^2 s_1 - \frac{1-\nu}{2}KA(f_1' + s_1) = 0 \\ -\frac{1-\nu}{2}KA(m^2\lambda^2 f_1 + m\lambda g_1) + \frac{1-\nu}{2}KA(f_1'' + s_1') + N_x m^2\lambda^2 f_1 = 0 \end{cases} \quad (14)$$

For solving the above system of equation it is necessary to assume

$$\begin{aligned}
\overline{T} &= 4\left(\frac{c}{a}\right)^3 - \left(\frac{b}{a}\right)^2\left(\frac{c}{a}\right)^2 - 18\frac{b}{a}\frac{c}{a}\frac{d}{a} + 27\left(\frac{d}{a}\right)^2 + 4\left(\frac{b}{a}\right)^3\frac{d}{a} \\
\overline{L} &= 36\frac{b}{a}\frac{c}{a} - 108\frac{d}{a} - 8\left(\frac{b}{a}\right)^3 \\
\overline{R} &= b/3a \\
\overline{Z} &= 3c/a - 9\overline{R}^2
\end{aligned} \tag{15}$$

where a, b, c and d are

$$\begin{aligned}
a &= \nu_1^2 R \\
b &= m^2\lambda^2(R(\nu_1^2(2\nu_2 - 1) - \nu_1 + \nu_2^2) + \xi\nu_1) - \nu_1^2 R^2 \\
c &= m^4\lambda^4(\xi(\nu_2^2 + 2\nu_1\nu_2 - 1) + R(\nu_1^2 + \nu_1 - \nu_1\nu_2^2 - \nu_1^2\nu_2)) + \\
&\quad m^2\lambda^2(R^2(4\nu_1^3 + 2\nu_1^2\nu_2) - R\xi(\nu_1^2 + \nu_1)) \\
d &= m^6\lambda^6(\xi\nu_1 - R\nu_1^2) + m^4\lambda^4(R\xi(\nu_1^2 + \nu_1) - R^2\nu_1^2) + m^2\lambda^2R^2\xi\nu_1^2
\end{aligned} \tag{16}$$

and

$$R = K\frac{A}{D}, \quad \xi = \frac{N_x}{D}, \quad \nu_1 = \frac{1-\nu}{2}, \quad \nu_2 = \nu \tag{17}$$

The solution of Equations (14) depends on whether $\overline{T} \geq 0$ or $\overline{T} < 0$. For example in the case of $\overline{T} < 0$, the equations are solved by assuming

$$\begin{aligned}
J_1 &= \frac{1}{3}\left(\overline{L}^2 - 432\overline{T}\right)^{\frac{1}{6}}\cos\left(\frac{1}{3}\arctan\left(\frac{12\sqrt{-3\overline{T}}}{\overline{L}}\right) + \chi\right) - \overline{R} \\
J_2 &= \left(\overline{L}^2 - 432\overline{T}\right)^{\frac{1}{6}}\left\{\begin{array}{l} -\frac{1}{6}\cos\left(\frac{1}{3}\arctan\left(\frac{12\sqrt{-3\overline{T}}}{\overline{L}}\right) + \chi\right) \\ -\frac{\sqrt{3}}{6}\sin\left(\frac{1}{3}\arctan\left(\frac{12\sqrt{-3\overline{T}}}{\overline{L}}\right) + \chi\right) \end{array}\right\} - \overline{R} \\
J_3 &= \left(\overline{L}^2 - 432\overline{T}\right)^{\frac{1}{6}}\left\{\begin{array}{l} -\frac{1}{6}\cos\left(\frac{1}{3}\arctan\left(\frac{12\sqrt{-3\overline{T}}}{\overline{L}}\right) + \chi\right) \\ +\frac{\sqrt{3}}{6}\sin\left(\frac{1}{3}\arctan\left(\frac{12\sqrt{-3\overline{T}}}{\overline{L}}\right) + \chi\right) \end{array}\right\} - \overline{R}
\end{aligned} \tag{18}$$

where $\chi = \begin{cases} 0 & \overline{L} \geq 0 \\ \frac{\pi}{3} & \overline{L} < 0 \end{cases}$

Now the solution depends on the sign of J_1, J_2 *and* J_3. For example in the case of $J_1 < 0, J_2 \geq 0, J_3 \geq 0$, the solution can be written as

$$
\begin{aligned}
&f_1(y) = C_f^1 \cos(\alpha y) + C_f^2 \sin(\alpha y) + C_f^3 \cosh(\beta y) + C_f^4 \sinh(\beta y) \\
&+ C_f^5 \cosh(\gamma y) + C_f^6 \sinh(\gamma y) \\
&g_1(y) = C_g^1 \cos(\alpha y) + C_g^2 \sin(\alpha y) + C_g^3 \cosh(\beta y) + C_g^4 \sinh(\beta y) \\
&+ C_g^5 \cosh(\gamma y) + C_g^6 \sinh(\gamma y) \\
&s_1(y) = C_s^1 \cos(\alpha y) + C_s^2 \sin(\alpha y) + C_s^3 \cosh(\beta y) + C_s^4 \sinh(\beta y) \\
&+ C_s^5 \cosh(\gamma y) + C_s^6 \sinh(\gamma y)
\end{aligned} \tag{19}
$$

where $\alpha = \sqrt{-J_1}$, $\beta = \sqrt{J_2}$, $\gamma = \sqrt{J_3}$ and $C_f^k, C_g^k, C_s^k \ (k = 1,..,6)$ denote unknown constants which depend on the displacement boundary conditions at edges $y = 0$ and b. The displacement boundary conditions for $f_1(y), g_1(y)$ and $s_1(y)$ at the edges $y = 0$ and b can be written as

$$
\begin{aligned}
&f_1(0) = \sqrt{2} w_{1i}, \qquad g_1(0) = \sqrt{2} \varphi_{x1i}, \qquad s_1(0) = \sqrt{2} \varphi_{y1i} \\
&f_1(b) = \sqrt{2} w_{1j}, \qquad g_1(b) = \sqrt{2} \varphi_{x1j}, \qquad s_1(b) = \sqrt{2} \varphi_{y1j}
\end{aligned} \tag{20}
$$

The buckling displacement amplitudes, which are depicted in Figure 1, can be written as the displacement vector:

$$
\underset{\sim}{\mathbf{d_1}} = \left\{ w_{1i},\ \varphi_{x1i}, \varphi_{y1i},\ w_{1j}, \varphi_{x1j}, \varphi_{y1j} \right\}^T \tag{21}
$$

Thus, the unknowns $C_f^k, C_g^k, C_s^k \ (k = 1,..,6)$ can be fully determined in terms of buckling displacement amplitudes and the solution of Equation (14) which satisfies the displacement boundary conditions of Equation (20) can be obtained analytically in terms of the edge displacements $\underset{\sim}{\mathbf{d_1}}$. By substituting the Equation (13) into Equation (11), the force boundary conditions for the moments and the resultant out-of-plane edge shear force as

$$
\begin{aligned}
&Q_{yi} = KA\nu_1 \left[\frac{\sqrt{2}}{2} f_1'(0) + \varphi_{y1i} \right] \quad Q_{yj} = -KA\nu_1 \left[\frac{\sqrt{2}}{2} f_1'(b) + \varphi_{y1j} \right] \\
&M_{yyi} = D \left[\frac{\sqrt{2}}{2} s_1'(0) - m\lambda\nu_2 \varphi_{x1i} \right] \quad M_{yyj} = -D \left[\frac{\sqrt{2}}{2} s_1'(b) - m\lambda\nu_2 \varphi_{x1j} \right] \\
&M_{xyi} = D\nu_1 \left[m\lambda\varphi_{y1i} + \frac{\sqrt{2}}{2} g_1'(0) \right] \quad M_{xyj} = -D\nu_1 \left[m\lambda\varphi_{y1j} + \frac{\sqrt{2}}{2} g_1'(b) \right]
\end{aligned} \tag{22}
$$

The left-hand sides of Equation (22) are the amplitudes of buckling force and moments at the corresponding edges of the strip and can be written as the force vector:

$$
\underset{\sim}{\mathbf{p_1}} = \left\{ Q_{1yi},\ M_{1xyi},\ M_{1yyi}, Q_{1yj},\ M_{1xyj}, M_{1yyj} \right\}^T \tag{23}
$$

The above equation can be re-arranged as

$$
\underset{\sim}{\mathbf{p}}_1 = \underset{\sim}{\mathbf{k}}_1 \underset{\sim}{\mathbf{d}}_1 \tag{24}
$$

where $\underset{\sim}{\mathbf{k}}_1$ denotes the strip out-of-plane stiffness matrix and is calculated

analytically. By applying these expressions to obtain the stiffness matrices of individual strips, the exact overall stiffness matrix $\underset{\sim}{\mathbf{K}}_1$ for the whole strips can be assembled by using the conventional routines of finite element analysis. The corresponding buckling problem can finally be expressed as the eigenvalue problem:

$$\underset{\sim}{\mathbf{K}}_1(N_x)\underset{\sim}{\mathbf{D}}_1=0 \tag{25}$$

where the vector $\underset{\sim}{\mathbf{D}}_1$ consists of the out-of-plane displacement amplitudes $(w_1,\varphi_{x1},\varphi_{y1})$ for each nodal line, and $\underset{\sim}{\mathbf{K}}_1$ is the stiffness matrix whose coefficients include trigonometric and hyperbolic functions involving longitudinal force N_x. It is realized that the application of exact method for buckling of structures has resulted in a transcendental eigenvalue problem in the form of Equation (25) as distinct from equation $(\underset{\sim}{\mathbf{K}}- N\underset{\sim}{\mathbf{K}}_G)\underset{\sim}{\mathbf{D}}=0$ which is encountered when approximate methods such as S-e FSM are used. In earlier publications by the authors [15-18], the Wittrick-Williams (W-W) algorithm is implemented in order to calculate the number of eigenvalues exceeded by any trial value of subjected force. However, this algorithm has been developed for analysing the plates and plate structures based on the classical plate theory while in the present study the first order shear deformation plate theory is applied. Thus, in order to resolve this problem the intervals which are found based on the CPT in Reference [18] have been updated. This is achieved by the knowledge that a thicker plate has a lower buckling coefficient. Thus, the given intervals in the case of CPT are altered until the determinants of the stiffness matrix for lower and upper ends of the interval become opposite in sign. This ensures that the updated interval consists of one eigenvalue for the thick plate.
In this paper, Bisection method [15-18] is selected as an iterative computational procedure to find the eigenvalues and eigenvectors.

2.3 Post-buckling analysis

Having obtained an exact shape of buckling deflection form, the analysis of post-buckling behaviour has proceeded on the assumption that the deflected form in the immediate post-buckling range is identical to that at the buckling, with only the deflection magnitudes varying. Thus, the post-buckling out-of-plane deflection function(w_2), the rotation of a transverse normal about the axis y (φ_{2x}) and the rotation of a transvers normal about the axis $x(\varphi_{2y})$ can be written as

$$w_2(x,y)=\delta w_1(x,y),\quad \varphi_{2x}(x,y)=\mu\varphi_{1x}(x,y),\quad \varphi_{2y}(x,y)=\xi\varphi_{1y}(x,y) \tag{26}$$

where δ, μ and ξ are the deflection and rotation coefficients. The in-plane boundary conditions at loaded ends of the strip are summarized as follows:

$$N_{xy}=0 \;\; at \;\; x=0 \; and \; L,\quad u_2=\begin{cases}0 & x=0\\ -\varepsilon L & x=L\end{cases} \tag{27}$$

By adopting the semi-energy post-buckling procedure in the manner described in Reference [17], the out-of-plane displacement w_2 is then substituted in the Von-Karman's compatibility equation (Equation(9b)) in order to find the corresponding in-plane displacement functions. It must be noted that since the only function that is used in the Von-Karman's compatibility equation is w_2 according to Equation (9b),

so the solution method of the equation will be the same as the method based on the CPT applied in Reference[17], but the only difference is in the form of the particular integral solution of the equation that is resulted from difference in deflection mode shape w_1. The in-plane displacement functions are found as follows:

$$u_2(x,y) = -\varepsilon x + \delta^2 f_{u_2}(y)\sin(2\lambda x) \tag{28}$$

$$v_2(x,y) = \nu\varepsilon y + \delta^2\left(g_{v_2}(y) + f_{v_2}(y)\cos(2\lambda x) - f_{v_2}(y)|_{y=0}\right) + v|_{x=y=0} \tag{29}$$

where

$$\begin{aligned} f_{u_2}(y) &= \frac{\lambda}{4}\left(\psi'' + 4\nu\lambda^2\psi - \frac{f_1(y)^2}{2}\right) \\ g_{v_2}(y) &= -\int_0^y \left(\frac{4\nu\lambda^2}{16} f_1(y)^2 + \frac{(f_1(y)')^2}{4}\right) \\ f_{v_2}(y) &= \frac{1}{8}(\psi''' - 4(2+\nu)\lambda^2\psi' + f_1(y)f_1(y)') \end{aligned} \tag{30}$$

and function $\psi = \psi(y)$ can be found from the following equation:

$$\psi'''' - 8\lambda^2\psi'' + 16\lambda^4\psi = (f_1(y)')^2 - f_1(y)f_1(y)'' \tag{31}$$

It is noted that the first term on the right-hand side of Equation (28) represents the prescribed uniform end-shortening strain. The amplitude of the second term, whilst divided by δ^2 and evaluated at $y = 0$ and b (i.e. $f_{u_2}|_{y=0}$; $f_{u_2}|_{y=b}$), represents the post-buckling in-plane displacement parameters u_{2i} and u_{2j}, respectively (see Figure 1). The first term on the right-hand side of Equation (29) describes the transverse in-plane expansion of the strip, which occurs due to Poisson's ratio effect. The second term describes the transvers in-plane movement of the longitudinal fibers of the strip. This movement, which is constant along the length of a given fiber, varies from a minimum value of zero at edge $y = 0$ to its maximum value at edge $y = b$. The third term describes the in-plane waviness of the longitudinal fibers. The amplitude of this term, whilst divided by δ^2 and evaluated at $y = 0$ and b (i.e. $f_{v_2}|_{y=0}$; $f_{v_2}|_{y=b}$), represents the post-buckling in-plane displacement parameters u_{2i} and u_{2j}, respectively (see Figure 1). Finally, the fourth term and the fifth term on the right-hand side of Equation (29) represent values which remain constant at all points on a given strip. It is also noted that the post-buckling in-plane displacements are a function of out-of plane buckling deflection mode (which is a function of critical longitudinal stress) and deflection coefficient δ.

Having obtained the in-plane displacements, the in-plane shear force and in-plane transverse force can be calculated from Equation (11). The outcome can be re-arranged to obtain the following set of linear simultaneous equations for the strip, which are designated as the strip stiffness equations:

$$\underset{\sim}{\mathbf{p}}_2 = \underset{\sim}{\mathbf{k}}_2 \underset{\sim}{\mathbf{d}}_2 + \underset{\sim}{\mathbf{f}}_2 \tag{32}$$

where

$$\underset{\sim}{\mathbf{d}}_2 = \begin{Bmatrix} u_{2i} & v_{2i} & u_{2j} & v_{2j} \end{Bmatrix}^T, \underset{\sim}{\mathbf{p}}_2 = \begin{Bmatrix} P_{2xi} & P_{2yi} & P_{2xj} & P_{2yj} \end{Bmatrix}^T \tag{33}$$

$\underset{\sim}{\mathbf{f}}_2$ consists of terms which correspond to the particular out-of-plane displacement

parameters (buckling displacement amplitudes $(w_1, \varphi_{x1}, \varphi_{y1})$), and $\underset{\sim}{\mathbf{k}}_2$ consists of terms which correspond to the in-plane displacement parameters (i.e. u_2, v_2) which is the stiffness matrix of the strip. Having developed the stiffness equations for each strip, the overall stiffness equations corresponding to the whole strips are formed by following the conventional finite element assembly procedure, and noting that the plate is not subjected to any external force, thus $\underset{\sim}{\mathbf{p}}_2$ vectors vanish during assembly process. The overall stiffness equations are

$$\underset{\sim}{\mathbf{K}}_2 \underset{\sim}{\mathbf{D}}_2 = \underset{\sim}{\mathbf{F}}_2 \tag{34}$$

where matrices $\underset{\sim}{\mathbf{K}}_2, \underset{\sim}{\mathbf{D}}_2$ and $\underset{\sim}{\mathbf{F}}_2$ are assembled from their counterparts for each strip. Once Equation (35) is solved and post-buckling in-plane displacement parameters are obtained, they are then substituted into Equations (28) and (29) to determine the analytical form of u_2 and v_2 for each strip, respectively. It is noted the obtained u_2 and v_2 and the assumed w_2, φ_{2x} and φ_{2y} are determined in terms of the deflection and rotations coefficients δ, μ and ξ, which will be calculated below.

2.4 Deflection and rotations coefficient (δ, μ and ξ) calculation

For a prescribed uniform end-shortening strain ε, the total strain energy of the plate $U = \sum U_s$ is simply equal to its total potential energy. By substituting Equations (26), (28) and (29) into Equations (2) and (7), and then by substituting the outcome into Equation (8) the strain energy of a single strip U_s is obtained. The summation of the strip strain energies gives the total strain energy of the plate as follows:

$$U = m_0 \varepsilon^2 + (R_1 - \varepsilon m_2)\delta^2 + R_2\delta\mu + R_3\delta\xi + R_4\mu^2 + R_5\mu\xi + R_6\xi^2 + m_4\delta^4 \tag{35}$$

where

$$R_1 = \sum \frac{L}{4}\int_0^b \left(KA\nu_1\lambda^2 f_1 f_1 + KA\nu_1 f_1' f_1'\right)\mathrm{d}y \quad R_5 = \sum \frac{L}{4}\int_0^b \left(2D\nu_1\lambda g_1' s_1 - 2D\nu_2\lambda g_1 s_1'\right)\mathrm{d}y$$

$$R_3 = \sum \frac{L}{4}\int_0^b \left(2KA\nu_1 f_1' s_1\right)\mathrm{d}y \quad R_4 = \sum \frac{L}{4}\int_0^b \left(KA\nu_1 g_1 g_1 + D\lambda^2 g_1 g_1 + D\nu_1 g_1' g_1'\right)\mathrm{d}y$$

$$R_2 = \sum \frac{L}{4}\int_0^b \left(2KA\nu_1\lambda f_1 g_1\right)\mathrm{d}y \quad R_6 = \sum \frac{L}{4}\int_0^b \left(KA\nu_1 s_1 s_1 + D s_1' s_1' + D\nu_1\lambda^2 s_1 s_1\right)\mathrm{d}y$$

$$m_0 = \sum \frac{1}{2A\nu_1} Lb \quad m_2 = \sum \frac{1}{4A\nu_1}\lambda^2 L\int_0^b f_1^2 \,\mathrm{d}y$$

$$m_2 = \sum \left\{ \left(\frac{1}{32}\mathrm{hEL}\lambda^4 \int_0^b \left(32\lambda^4\psi^2 + 16\lambda^2\psi'^2 + 2\psi''^2 + f_1^4\right)\mathrm{d}y \right) + \frac{1}{2} LD\lambda^2\nu_2 (f_1 f_1')\Big|_0^b \right\} \tag{36}$$

In Equations (36) the summation relates to all strips. All the integrations in above equation are determined analytically to determine the constants. It is worth to be emphasized that the whole constants are evaluated once. It is noted that the deflection and rotations coefficients are the only unknowns in the energy expression.

The strain energy is then minimized by differentiating U with respect to δ, μ and ξ. This gives

$$\begin{aligned}
\frac{\mathrm{d}U}{\mathrm{d}\delta} &= 4m_4\delta^3 + 2(R_1 - \varepsilon m_2)\delta + R_2\mu + R_3\xi = 0 \\
\frac{\mathrm{d}U}{\mathrm{d}\mu} &= R_2\delta + 2R_4\mu + R_5\xi = 0 \\
\frac{\mathrm{d}U}{\mathrm{d}\xi} &= R_3\delta + R_5\mu + 2R_6\xi = 0
\end{aligned} \tag{37}$$

It is noted that in Equation (38) , $\xi = \mu = \delta = 0$ is a trivial equilibrium path, and thus the branched equilibrium path is obtained

$$\begin{aligned}
\delta &= \pm\sqrt{\frac{R_2^2R_6 + R_3^2R_4 + R_5^2R_1 - R_2R_3R_5 - 4R_1R_4R_6 + m_2\varepsilon(4R_4R_6 - R_5^2)}{2m_4(4R_4R_6 - R_5^2)}} \\
\mu &= -\delta\frac{2R_2R_6 - R_3R_5}{4R_4R_6 - R_5^2} \\
\xi &= \delta\frac{R_2R_5 - 2R_3R_4}{4R_4R_6 - R_5^2}
\end{aligned} \tag{38}$$

The longitudinal mid-plane stress σ_x can be obtained as the following equation:

$$\sigma_x = -E\varepsilon + \frac{E\lambda^2\delta^2}{4}(f_1^2 + 2\psi''\cos(2\lambda x)) \tag{39}$$

The longitudinal force/load acting on a strip is determined by integrating the longitudinal mid-plane stresses σ_x over the strip cross-sectional area. The total longitudinal force/load acting on a plate at a given cross-section along the plate length, corresponding to a prescribed end-shortening strain, is obtained by summation of all strip forces at the same cross-section, i.e.

$$P = \sum P_s = E\varepsilon\sum bt - \frac{E\lambda^2\delta^2}{4}\sum t\int_0^b (f_1^2 + 2\psi''\cos(2\lambda x))\,dy \tag{40}$$

By substituting the deflection coefficient from Equation (38) into Equation (40) and simplifying the result

$$\begin{aligned}
P = E\varepsilon\left(\sum bt - \frac{\lambda^2 m_2}{8m_4}\sum t\int_0^b (f_1^2 + 2\psi''\cos(2\lambda x))\,dy\right) \\
+ \frac{1}{L}\frac{m_2}{2m_4}\left(R_1 + \frac{R_2R_3R_5 - R_2^2R_6 - R_3^2R_4}{4R_4R_6 - R_5^2}\right)
\end{aligned} \tag{41}$$

It is obvious that the $P - \varepsilon$ relationship in the post-buckling region is a linear function which is tangent to the actual post-buckling curve at the buckling point. The slope of this line, which is post-buckling stiffness S^*, can be obtained by differentiating Equation (41) with respect to ε. The effective pre-buckling stiffness S can be obtained by letting $\delta = 0$ in Equation (40) and differentiating the equation with respect to ε. Therefore, the relative post-buckling stiffness defined as the ratio of the post-buckling stiffness to the pre-buckling stiffness can be calculated from equation (42) in a very straightforward manner

$$\frac{S^*}{S} = 1 - \frac{\lambda^2 m_2}{8 m_4 \sum bt} \sum t \int_0^b (f_1^2 + 2\psi'' \cos(2\lambda x))\, dy \tag{42}$$

where $\sum bt$ is the cross-sectional area of the plate.

3 Results and discussions

This section presents a number of numerical examples showing the excellent performance of the proposed algorithm, which was implemented in a Maple 11 program. It is noted that the program is run on a standard Core 2 Dou 2.40 GHz PC. The results of the developed F-a FSM based on the FSDT in buckling phase as well as post-buckling region are compared with those of F-a FSM based on the CPT which are carried out by first two authors of this paper [18].

In order to investigate the verification of the proposed method, some representative plates with various boundary conditions are considered and each plate is divided into two, four, ten and fifty strips of equal length giving four cases for consideration. The investigation of the results has revealed that the critical buckling load, the relative stiffness values and the post-buckling results are identical among the four cases as expected. Thus, each plate can be accurately modelled by only one strip to it. It may be noted that the Poisson's ratio ν is assumed to be equal to 0.3 for the entirety of this paper and in the whole examples it is assumed that the plate buckles with one half-length wave along the x direction.

3.1 Buckling results

In presenting the results the non-dimensional plate buckling coefficient is introduced as $k = N_x b^2 / \pi^2 D$. Table 1 represents the numerical values of buckling coefficient obtained by the developed method (F-a FSM based on the FSDT) for various plate thicknesses, as well as the F-a FSM based on the CPT [18]. Out-of-plane boundary conditions and the aspect ratio ($\varphi = L/b$) of the plates under consideration are also represented in this table.

Buckling coefficient(k)									
Case	Edges BCs	φ (L/b)	L/h						CPT[18]
			5	10	15	25	50	100	
1	S-S	1	3.26373	3.78645	3.90219	3.96423	3.99100	3.99775	4.00000
2	C-S	1	4.15097	5.22317	5.49591	5.64912	5.71704	5.73438	5.74021
3	C-F	2	0.91992	1.17042	1.24414	1.29193	1.31868	1.32859	1.33598

S, C and F denote simply-supported, clamped and free respectively.

Table 1. The minimum plate buckling coefficient obtained by the developed method

The table shows that in each case as the thickness of the plate decreases, the buckling coefficient converges to that obtained by using the CPT. For example in

the case 1 the buckling coefficient value converges to the well-known buckling coefficient value of 4.0 for classic plates.
Figure 2 is made from the data of case 1 in Table 1.This results show that the classical plate theory (CPT) loses its validity as the length to thickness ratio decreases.

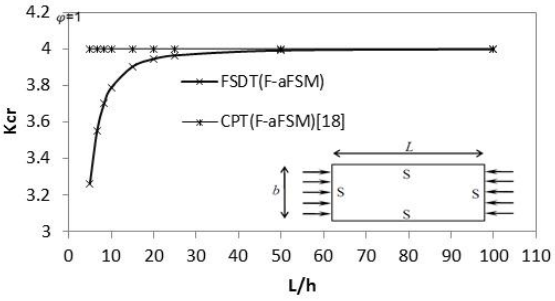

Figure 2. Buckling coefficients for a square simply supported plate.

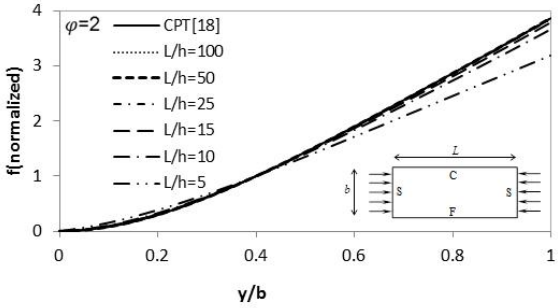

Figure 3. Out-of-plane deflection modes for various thicknesses for a C-F plate.

Finally, the buckling mode shapes for a C-F plate (case 3 in Table 1) are depicted in Figure 3. As it is seen in the figure, for thin plates there is a very good agreement between the mode shapes obtained by both F-a FSM, based on either the FSDT or CPT.

3.2 Relative stiffness and initial post-buckling behaviour

Table 2 represents the numerical values of the relative stiffness (i.e., the S^*/S at the instant of buckling) for various plates with various out-of-plane boundary conditions. The transverse in-plane displacement is allowed at the edges of the plate. The presented values consist of those derived from the developed F-a FSM analysis based on FSDT and those presented in Reference [18], which have been calculated by implementing the F-a FSM based on CPT. The numerical values of the relative stiffness obtained by the developed F-a FSM analysis are exact because the deflected form in the immediate post-buckling range is identical to that at the buckling.

Relative Stiffness(S*/S)										
Case	Unloaded edges BCs	φ (L/b)	CPT[18]	L/h						
				200	100	50	25	15	10	5
1	S-S	1	0.408336	0.408336	0.408336	0.408336	0.408336	0.408336	0.408336	0.408336
2	C-S	1	0.494057	0.494025	0.493930	0.493554	0.492090	0.488819	0.483066	0.461289
3	C-F	2	0.556664	0.556963	0.557167	0.557298	0.556495	0.553410	0.546843	0.516499

Table 2.The plate relative stiffness obtained by the developed method

The table shows that as the thickness decreases, the values of relative stiffness obtained by F-a FSM based on FSDT converge to those values from F-a FSM based on CPT. It can be seen that the relative stiffness for a S-S plate does not change as the thickness changes.
The initial post-buckling behaviour for a C-F plate is shown in Figure 4.

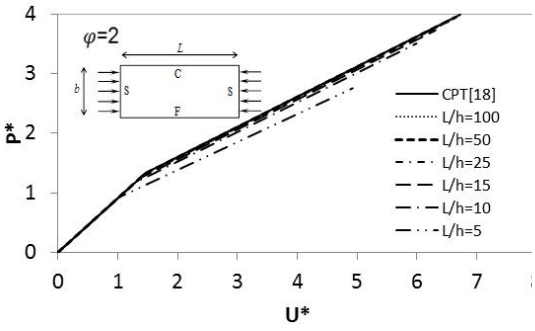

Figure 4. Load-end shortening plot for a C-F isotropic plate

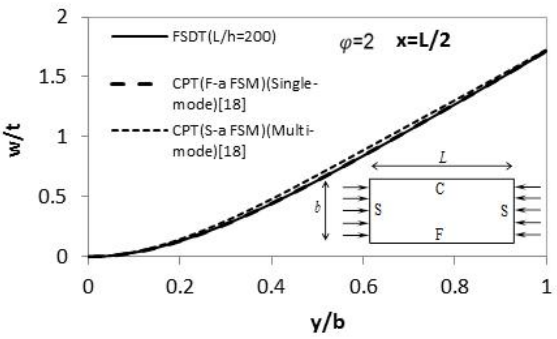

Figure 5. Out-of-plane deflection for a thin C-F plate.

Figure 5 shows the out-of-plane deflection of the preceding plate with $L/h = 200$ when it is subjected to a load $P = 1.5\,P_{Cr}$. As depicted in the figure the current FSDT deflection variation, which is effectively obtained based on a single mode of buckling, is similar to that obtained by CPT single-mode F-a FSM.

4 Conclusion

Theoretical developments of an exact finite strip for the buckling and initial post-buckling of moderately thick plates have been presented. Each plate has been modelled by assigning the developed exact strip across its width. The transcendental overall stiffness matrix for the whole plate has been obtained by assembling the individual strip stiffness. The presented buckling results have indicated the capability of the developed F-a FSM analysis based on the FSDT in terms of delivering exact results at the buckling point. The values of the relative post-buckling stiffness obtained by the developed F-a FSM analysis are also extremely accurate at the buckling point because the exact buckling mode shape and corresponding buckling coefficient are used in the post-buckling analysis. Having compared the F-a FSM results with those from S-a FSM inside the post-buckling range, a small difference between the results is experienced. This has been due to the fact that the current F-a FSM analysis utilizes only a single mode to represent the out-of-plane deflection of the plates in the post-buckling region. However, for a given degree of accuracy in the results, the F-a FSM analysis requires less computational effort, as a consequence of implementing less degrees of freedom, compared to the S-a FSM. Finally, it is worth mentioning that the promising results obtained in the current paper have made the authors to extend the formulation of

single-term F-a FSM to the multi term F-a FSM. Some interesting results have already been obtained which will be published once the investigation is complete.

References

[1] Y.K. Cheung, "Finite strip method in structural analysis", Pergamon press, p.26,1976.

[2] T.R. Graves-Smith ,S. Sridharan ,"A finite strip method for buckling of plate structures under arbitrary loading." Int J Mech Sci,20,685–93,1978.

[3] S.C.W. Lau, G.J. Hancock ,"Buckling of thin flat-walled structures by a spline finite strip method", Thin-Walled Struct,4,269–94,1986.

[4] S. Wang, D.J. Dawe, "Buckling of composite shell structures using the spline finite strip method", Composites B, ,30,351–64,1999.

[5] G.P. Zou ,S.S.E. Lam, "Buckling analysis of composite laminates under end shortening by higher-order shear deformable finite strips", Int J Numer Methods Eng,55,1239–54,2002.

[6] T.R. Graves-Smith, S. Sridharan, "A finite strip method for the post-locally buckled analysis of plate structures", Int J Mech Sci,20,833–42,1978.

[7] S. Sridharan, T.R. Graves-Smith, "Post-buckling analyses with finite strips", J Eng Mech (ASCE),107,869–88,1981.

[8] J. Rhodes, J.M. Harvey," Examination of plate post-buckling behaviour", J Eng Mech (ASCE),103(EM3),461–78,1977.

[9] K. Marguerre, "The apparent width of plates in compression", NACA technical memorandum, No. 833, National Advisory Committee for Aeronautics, Washington, DC, 1937.

[10] J. Rhodes, "Research into thin-walled structures at the University of Strathclyde– a brief history", In: The conference proceedings of Bicentenary conference onthin-walled structure, University of Strathclyde, UK; 2nd–4th December 1996.

[11] S.M. Chou, J. Rhodes, "Review and compilation of experimental results on thin walled structures" Comput Struct,65(1),47–67,1997.

[12] H.R. Ovesy, J. Loughlan, S.A.M. Ghannadpour," Geometric non-linear analysis of thin flat plates under end shortening, using different versions of the finite strip method", Int J Mech Sci,47,1923–48,2005.

[13] H.R. Ovesy, J. Loughlan, S.A.M. Ghannadpour," Geometric non-linear analysis of channel sections under end shortening, using different versions of the finite strip method", Comput Struct,84,855–72,2006.

[14] H.R. Ovesy, J. Loughlan, S.A.M. Ghannadpour, G. Morada, " Geometric non-linear analysis of box sections under end shortening, using three different versions of the finite strip method" Thin-Walled Struct,44,623–37,2006.

[15] S.A.M. Ghannadpour, H.R. Ovesy, "An exact finite strip for the calculation of relative post-buckling stiffnessof I-section struts", International Journal of Mechanical Sciences,50,1354-1364,2008.

[16] S.A.M. Ghannadpour, H.R. Ovesy, “The application of an exact finite strip to the buckling of symmetrically laminated composite rectangular plates and prismatic plate structures”, Composite Structures,89,151-158,2009
[17] H.R. Ovesy, S.A.M. Ghannadpour, ”An exact finite strip for the initial postbuckling analysis of channel section struts”, Computers and Structures,89,1785–1796,2011.
[18] H.R. Ovesy, S.A.M. Ghannadpour,” An exact finite strip for the calculation of relative post-buckling stiffness of isotropic plates”, Structural Engineering and Mechanics,31,181-210,2009.